IEEE Access
Multidisciplinary | Rapid Review | Open Access Journal

Received December 11, 2019, accepted December 18, 2019, date of publication December 23, 2019,
date of current version December 31, 2019.

Digital Object Identifier 10.1109/ACCESS.2019.2961565

K-State Resonators for High-Coding-Capacity Chipless RFID Applications

WAZIE M. ABDULKAWI AND ABDEL-FATTAH A. SHETA
Department of Electrical Engineering, King Saud University, Riyadh 11421, Saudi Arabia

Corresponding author: Wazie M. Abdulkawi (walkadri@ksu.edu.sa)

This work was supported by the Deanship of the Scientific Research and the Graduate Students Research Support (GSR), King Saud University, Riyadh, Saudi Arabia.

ABSTRACT This paper presents a new, compact, high-coding-capacity resonator suitable for applications in chipless RFID tags. These tags consist of multiple resonators and two cross-polarized ultra-wide band antennas. Each resonator contains a U-shaped coupled microstrip frame with isolated (K-1) legs inside. One of the legs is designed to be connected to the U-frame via a metallic strip in order to adjust its resonance frequency. Using this feature, the frequency of each resonator can be reconfigured to be equal to one of the K-resonance frequencies. Therefore, each resonance presents one of the K-states of the resonator. This allows each resonator to represent more than one bit of information; this arrangement also permits N resonators tags to provide K^N codes. The structure can store large volumes of data in a small area and can simplify the detection process by only reading N resonance frequencies for each code. When N resonator tags are used in the proposed structure, the amount of data that can be encoded increases to $2^{(\log K/\log 2)N}$ compared to 2^N in the case of conventional one-bit resonator (2-states) tags. An additional arrangement is also proposed and investigated in order to improve the spectral efficiency by allowing the bandwidth of each single resonator to be shared between two resonators. Several tags for codes with $K = 8$ are designed and implemented on the RT Duroid 5880 substrate as a proof-of-concept. An 8-state of the proposed resonator can be implemented in an area that is almost the same size as the area of a conventional 2-state resonator operating at 5 GHz. A satisfactory agreement between the empirical and simulated results is then confirmed.

INDEX TERMS K-state resonator, high coding capacity, chipless RFID, ultra-wideband antenna (UWB), Internet of Things (IoT).

I. INTRODUCTION

Radio frequency identification (RFID) technologies are being considered as replacements for barcodes due to the serious limitations of the latter, including a low capacity, an inadequate detection range, and line of sight requirements. RFID systems use radio frequency waves for object identification. They are found in various applications, including item tracking, industrial robotics, wireless sensors (internet of things), smart cards, etc. [1], [2]. Conventional RFID tags utilize integrated circuit (IC) chips that limit the applicability of RFID tags due to their prohibitive costs. Chipless RFID tags have been recently proposed to reduce the cost of the tags by removing the expensive IC chip, and thus producing tags with fully printable structures. However, chipless RFID tags are limited by their sizes and data capacities. These parameters are still not competitive compared to the small sizes and high memory storage capacities of silicon ICs.

In recent years, several approaches have been suggested to alleviate the aforementioned limitations. Two primary methods are commonly used in data encoding for chipless RFID tags — the time-domain system and the spectral signature system (or frequency domain-based system). In time-domain-based tags [3]–[5], the reader broadcasts short pulses and receives the echoes from the tags with specific time delays corresponding to the tag information. Although time-domain tags have smaller response times compared to frequency-domain tags, their bit encoding capabilities are limited for practical implementation because of the requirements of large delay lines or very narrow

The associate editor coordinating the review of this manuscript and approving it for publication was Renato Ferrero.

pulses. Therefore, most of the research on how to reduce the size and increase the data capacity of chipless RFID tags is based on the frequency-domain approach. In this case, encoding is performed using resonant elements adjusted to specific frequencies within the system's operating bandwidth.

The presence or absence of resonance corresponds to the values 1 or 0 in the logic, respectively. In the frequency-domain chipless RFID technique [6]–[9], the reader transmits the RF signals within the tags' spectrums of operation and receives the retransmitted or backscattered signals from the tags. The tags are then divided into two categories based on the response received — the backscattered type [10]–[19] and the retransmission type [20]–[23]. In backscattering-based tags, separate antennas are not required for transmitting the interrogatory signal or receiving the backscattered response. This technique has the advantages of a small tag size and an easier readability. However, the number of available bits is limited and adding more bits introduces coupling, thereby affecting the resonance frequencies of other units. More extensive calibration may be required to overcome this limitation [24]—[26]. A retransmission-based chipless RFID tag consists of two cross-polarized antennas and a sequence of resonators where the information is stored [22], [27]. This technique exhibits a more stable performance because the use of two orthogonally polarized antennas significantly reduces the interference between the transmitted and received waves. Moreover, the tag capacity can be increased by simply adding more resonators to the structure and the resultant mutual coupling can be reduced by adjusting the distance between the resonators [28]–[30]. Several chipless RFID tags have been developed based on two-state (1 bit) resonators [31]–[37]. The authors of [38], [39] presented spiral resonators to encode the data into a spectral signature. They began with six spiral resonators to encode 6 bits and progressed to encoding 35 bits using 35 resonators in the range of 3-7 GHz. Two orthogonal monopole antennas were then used to receive and retransmit the interrogatory signals with a small amount of mutual coupling between them. Other 1 bit resonators, such as open stub [31], open loop [33], L-shaped [36], and the complementary split ring resonator [37] have been investigated for chipless RFID applications. An improved structure was proposed in [40], [41] that combines a spiral and T-shaped coupled line in a compact form. Each resonator in these configurations is represented by only one bit. Hence, an n-bit tag requires n resonators and produces 2^n codes.

In frequency-based tags, the number of available bits is given by the number of resonators. To improve the bit capacity without increasing the number of resonators two approaches have been suggested — multi-state-resonator chipless RFID tags [30], [42]–[44] and hybrid-domain-based chipless RFID tags [45]–[48]. In hybrid chipless RFID tags, the multi-domain technique is used to increase the capacity of each resonator to more than one bit. However, the hybrid domain is still required for a high spectral bandwidth and the configuration is not suitable for low-cost applications [49]. In multi-state-resonator tags each resonator can have more than two states. In [50], [51], the authors proposed multi-mode stepped impedance resonators and discussed their application in chipless RFID tags. Two sets of transmission lines were used to realize the multi-mode resonators. The proposed tags used exciter and detector probes instead of the receiver and transmitter antennas used by conventional tags. However, the tag size was reduced during the set-up, with the detection area limited to less than a few millimetres. The performance of chipless RFID tags is not only defined by its encoding capacity (bits/cm^2/GHz) but also by other parameters as defined in [52], [53], such as; spectral capacity (bits/GHz), spatial density (bits/cm^2), spatial density at the centre frequency (bits/λ^2), encoding capacity at the centre frequency (bits/λ^2/GHz), and the overall size (mm^2). Table 1 shows the performance comparison for previously published tags in the frequency domain, backscattered and retransmission-based techniques. In this table, two of the proposed structures exhibit a high performance in relation to the retransmitted-based chipless RFID transponders and are thus included.

In this paper, a new K-state resonator is proposed for compact high-coding-capacity chipless RFID tags. This tag is comprised of N resonators and each resonator is equipped with (K-1) arms. Each resonator can be tuned to present one of the K possible resonance frequencies. Therefore, the tag can be reconfigured to produce K^N codes and K×N possible resonance frequencies. The chipless RFID reader only needs to read N frequencies for each code. The difference between each two adjacent resonance frequencies is approximately 100 MHz. Therefore, a large bandwidth is required for each resonator and a limited data capacity is expected from a tag within a given bandwidth [54]. This drawback can be alleviated by decreasing the difference between the adjacent resonance frequencies and allowing each two resonators to share the same frequency band. Three different configurations with $K = 8$ are designed and then investigated as proofs-of-concept. The first configuration consists of four resonators operating in the range of 4.4 GHz to approximately 8 GHz. The second configuration is proposed to increase the coding density and to reduce the required bandwidth. The third configuration consists of 6 resonators arranged specifically to increase the spectral efficiency. These configurations are then designed, fabricated, and evaluated. The proposed configurations are designed and fabricated on the RT Duroid 5880 substrate ($\varepsilon_r = 2.2$, $\tan\sigma = 0.0009$, and $h = 0.79$ mm). The measured results agree well with the simulated ones. The proposed technique allows for storing a large amount of data in a compact space in order to reduce the cost of storage per bit.

The remainder of this paper is organized as follows. Section 2 introduces and describes the proposed resonator. The multi-resonator structures for chipless RFID tags are analysed and discussed in Section 3. Additionally, three different configurations are designed and experimentally

TABLE 1. Comparison between the proposed tag and different frequency domain chipless RFID tags.

Resonator type	Frequency band (GHz)	Capacity (bits)	Spectral capacity (bits/GHz)	Spatial density (bits/cm^2)	Spatial density at the centre frequency (bits/λ^2)	Encoding capacity (bits/cm^2/GHz)	Encoding capacity at the centre frequency (bits/λ^2/GHz)	Size (mm^2)
Backscattered-based								
Loaded dipoles [16]	1.8-3.6	20	11.11	0.66	81.51	0.37	45.28	55×55
Dipole array [52]	2.2-3.5	20	15.38	0.56	61.47	0.43	47.28	60×60
Log-periodic dipole [55]	2-12	7	0.7	0.09	1.68	0.01	0.17	87.4×87.4
Crossed dipoles [56]	2-5	4	1.33	0.2	14.49	0.07	4.83	45×45
Slotted-I [12]	6-12	18	3	4.08	45.29	0.68	7.55	21×21
Slotted-U [13]	2-4	20	10	0.77	76.82	0.39	38.41	50×52
Slotted-I [19]	3-7	6	1.5	0.38	13.48	0.1	3.37	40×40
Slotted-L [57]	3-6	8	2.67	2	88.76	0.67	29.59	20×20
Slotted-U [58]	7-12	8	1.6	3.13	31.13	0.63	6.23	16×16
Slotted-delta [59]	3-10	18	2.57	2.11	44.98	0.30	6.43	31.35×27.15
Concentric ring [17]	3-13	4	0.4	2.04	28.65	0.20	2.87	14×14
Loaded ring [48]	3-9	23.7	3.96	2.63	49.97	0.44	8.33	30×30
Nested scatterers [18]	4-7.5	6	1.71	2.67	72.5	0.76	20.71	15×15
C-strips [10]	2-4	20	10	1.14	114.13	0.57	57.07	70×25
C-strips [15]	2-4	20	10	1.10	109.74	0.55	54.87	70×26
C-strips [24]	2-5	5	1.67	0.33	25	0.11	8.33	50×30
Inverted-M strips [14]	3-8	20	4	15.15	412.69	3.03	82.54	12×12
Retransmitted-based								
Spiral [20]	3-7	35	8.8	0.6	22	0.15	5.5	88×65
Spiral [21]	5-11	23	3.8	0.33	4.67	0.06	0.78	108×64
Spiral [41]	2-3	3	3	0.03	4.35	0.03	4.35	124×80
Stub [23]	2-4	10	5	0.12	12.1	0.06	6.05	110×75
Open stubs [31]	1.9-2.5	8	3.08	0.17	14.63	0.07	5.63	80×60
Open stubs [32]	4-9	16	3.2	0.24	5.16	0.05	1.03	110×60
Open loop [33]	3-6	8	2.67	0.25	11.11	0.08	3.7	84.84×37.8
L-strips [36]	4.8-10.93	20	3.26	0.92	13.33	0.15	2.17	50×43.22
Coupled-line [30]	5-8.2	12	3.75	0.82	16.95	0.26	5.30	55.65×26.25
Coupled-line [44]	5-8	21	7	0.16	3.43	0.05	1.14	147.4×87.1
Complementary split ring [37]	4-5.5	6	4	0.09	3.78	0.06	2.52	115×55
The proposed tag (retransmitted-based)								
Un equally arms with K=8, and N=6 (Fig. 14)	4.2-8.3	18	4.39	1.07	24.66	0.30	6.01	54.51×30.92
Same bandwidth shared between two identical resonators with K=8, and N=12 (Fig. 19)	4.2-8.3	31.26	7.62	1.31	30.06	0.36	7.33	77.34×30.92

validated. In Section 4, several chipless RFID tags based on the 8-state resonator are discussed, designed and experimentally tested. Finally, conclusions are drawn in Section 5.

II. DESIGN AND DESCRIPTION

As previously mentioned, the cost of a chipless RFID tag is mostly determined by its size. This paper proposes a new

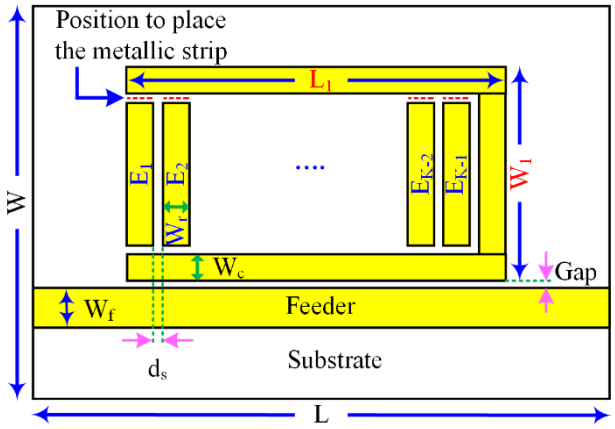

FIGURE 1. Top view of the proposed K-states microstrip resonator's geometry.

structure for resonators to increase the number of available bits per resonator, thus increasing the data capacity and decreasing the physical area required. The proposed tag structure was comprised of N microstrip resonators and each resonator was equipped with (K-1) elements or arms, as depicted in Fig. 1. The main advantages of this resonator are the higher bit encoding capacity and the smaller tag size. Each resonator can be adjusted to resonate at one specific resonance frequency out of the K possible frequencies. Thus, a tag consisting of N resonators provides K×N possible frequencies with N resonant frequencies corresponding to each code. Therefore, the tag can be reconfigured for K^N codes, while the reader merely needs to read N-frequencies.

In general, for K states/resonators and N resonators, the amount of data that can be encoded is K^N, which is equivalent in a binary system to 2^x, where x is given by x= N(log k/log 2). Therefore, the amount of data that can be encoded increases to $2^{(\log K/\log 2)N}$ compared to 2^N in the case of conventional one-bit resonator (2-state) tags.

As an example, if N = 4 and K = 8, the proposed structure can provide (K^N) 4096 codes, while the bi-state resonator structure can only provide 16 codes using 4 resonators.

For K = 8, each resonator consists of seven arms, (E_1 to E_7, as K − 1 = 7). A coupled transmission line placed very close to the feeder is studied as a proof-of-concept. Any of the arms can be connected to the coupled line by a small metallic strip. When connected to the coupled line, E_1 to E_7 produce corresponding resonance frequencies, denoted by f_1 to f_7, respectively. If each element is not connected, the resonator resonates at frequency f_8. Table 2 records the dimensions of the resonator designed on the RT Duroid 5880 substrate with a dielectric constant of 2.2, a loss tangent of 0.0009, and a thickness of 0.78 mm. The structure depicted in Fig. 1 is simulated using an electromagnetic simulator either by not connecting any of the arms to the coupled line, thereby producing a resonance frequency f_8, or by connecting only one of the 7 arms to the coupled line, thereby producing a resonance frequency from f_1 to f_7.

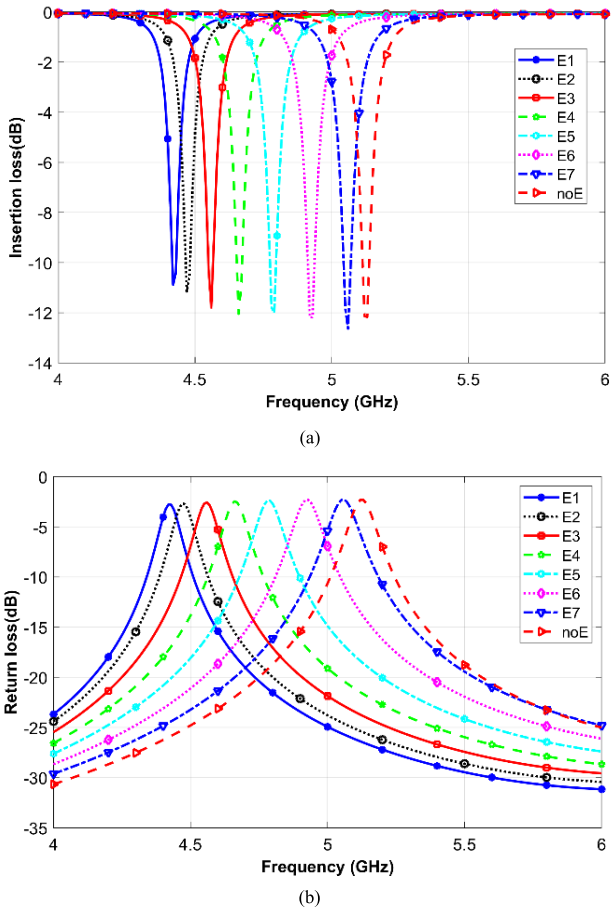

FIGURE 2. S21 and S11 responses for the 8-state single resonator structure (K = 8, N = 1).

TABLE 2. Dimensions of the proposed tag.

Parameter	Description	Physical value (mm)
L	Proposed tag length	19.4
W	Proposed tag width	8.1
L_l	Spiral resonator length	9.4
W_l	Spiral resonator width	5.5
W_r	Element width	1
W_c	Coupled line width	1
W_f	Feeder width	2.4
Gap	Gap between the resonator and the microstrip feed line	0.2
d_s	Separation between two arms of the resonator	0.3

The simulated S_{21} (insertion loss) and S_{11} (return loss) are presented in Fig. 2, and the resultant resonant frequencies corresponding to each statistic are summarized in Table 3. From these results, it is evident that there are eight distinct resonant nulls in the magnitude of the S_{21} and 8-peaks in S_{11}, since the structure represents the stopband filter characteristics. The dimensions presented in Table 2 are optimized to resonate at any of the eight resonant frequencies, from f_1 to f_8, as shown in Table 3.

TABLE 3. Possible resonant frequencies and their corresponding codes for a single resonator.

State	Element connected to frame	Identifier	Frequency (GHz)	RFID Code
1	E_1	f_1	4.42	000
2	E_2	f_2	4.47	001
3	E_3	f_3	4.56	010
4	E_4	f_4	4.66	011
5	E_5	f_5	4.79	100
6	E_6	f_6	4.93	101
7	E_7	f_7	5.10	110
8	None	f_8	5.13	111

TABLE 4. All possible frequencies in GHz for the four multi-resonators.

f_1	f_2	f_3	f_4	f_5	f_6	f_7	f_8
4.42	4.47	4.56	4.66	4.79	4.93	5.10	5.13
f_9	f_{10}	f_{11}	f_{12}	f_{13}	f_{14}	f_{15}	f_{16}
5.17	5.22	5.30	5.40	5.53	5.67	5.85	5.90
f_{17}	f_{18}	f_{19}	f_{20}	f_{21}	f_{22}	f_{23}	f_{24}
5.94	6.01	6.12	6.25	6.41	6.60	6.82	6.91
f_{25}	f_{26}	f_{27}	f_{28}	f_{29}	f_{30}	f_{31}	f_{32}
7.00	7.06	7.16	7.29	7.44	7.61	7.81	7.88

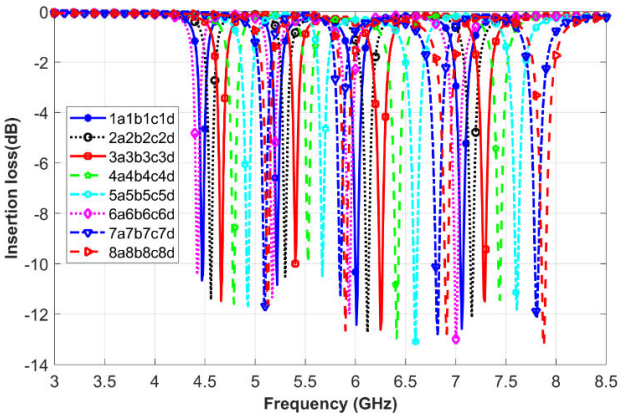

FIGURE 3. S_{21} response for the four 8-states resonators (K = 8, N = 4).

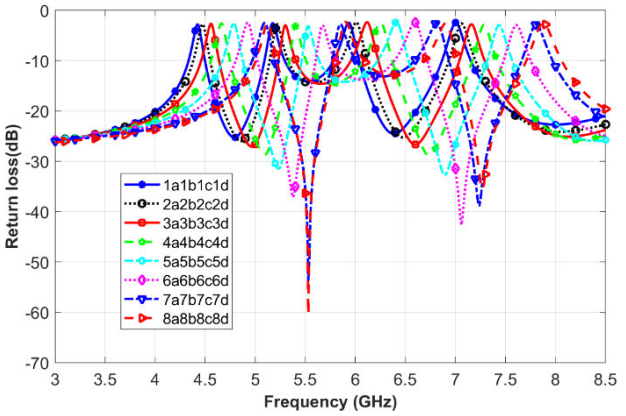

FIGURE 4. S_{11} response for the four 8-state resonators (K = 8, N = 4).

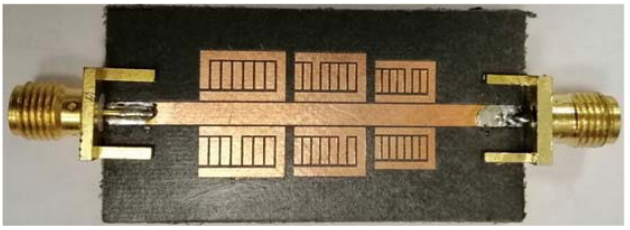

FIGURE 5. Photograph of the fabricated tag ($f_1 f_4 f_{11} f_{14} f_{21} f_{24}$).

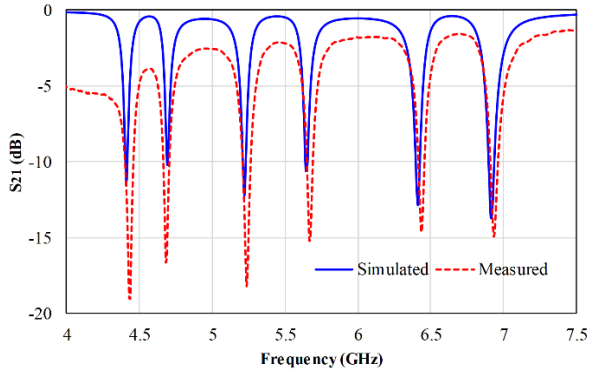

FIGURE 6. Tag response ($f_1 f_4 f_{11} f_{14} f_{21} f_{24}$).

When an arm is connected to the coupled line it is said to be active, and it is called passive if it is kept unconnected. In this configuration, each resonator can be configured to represent one of 8 different states or, in other words, each resonator can encode 3 bits of information. More bits can be encoded by adding more arms.

III. TWO-PORT MULTI-RESONANT STRUCTURES

To validate the concept via experiments, a tag resonant element consisting of 4 resonators (N = 4) is designed on the same dielectric material as the resonator discussed in the preceding section. K is set to 8, thus making the number of possible codes equal to $8^4(2^{12})$. Each code can be uniquely described using only 4 of the 32 possible resonant frequencies. The complete set of possible frequencies is listed in Table 4. The simulated S_{21} and S_{11} responses for each possible frequency are superimposed in Fig. 3 and Fig. 4, respectively. Four frequencies are read simultaneously using the RFID reader. Although the coding capacity increases in this example, the required bandwidth is 3.46 GHz, with each resonator (3-bit) requiring approximately 865 MHz. This is quite high, and it reduces the tag's spectral efficiency (1 bit/290 MHz). Consequently, two approaches are suggested in this paper to increase the spectral efficiency. The first technique is to allow the same bandwidth to be shared between the two resonators, and the second technique reduces the difference between adjacent frequencies to approximately 70 MHz and optimizes the structure in order to clearly read any code, especially those corresponding to adjacent resonances. Both techniques can significantly reduce the required bandwidth and improve the spectral efficiency.

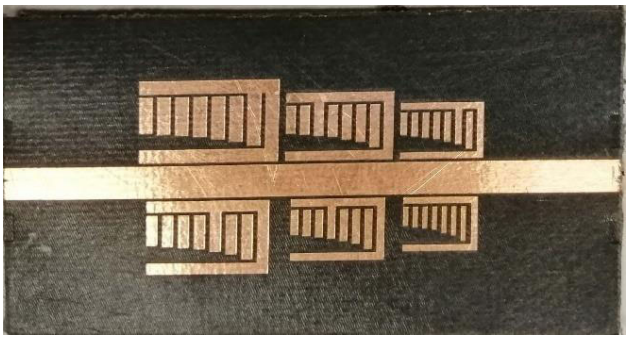

(a)

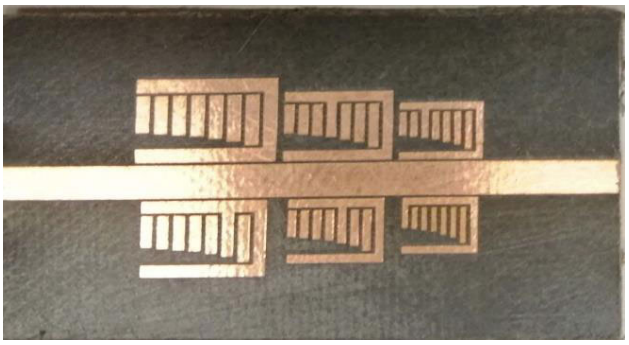

(b)

FIGURE 7. Photographs of the fabricated tags (a) $f_7f_{13}f_{19}f_{28}f_{38}f_{48}$ and (b) $f_8f_{14}f_{20}f_{29}f_{35}f_{41}$.

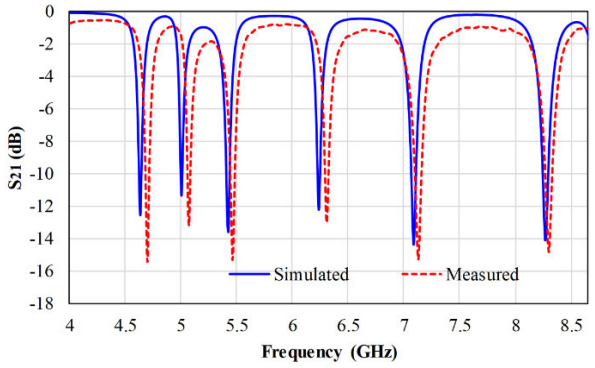

(a)

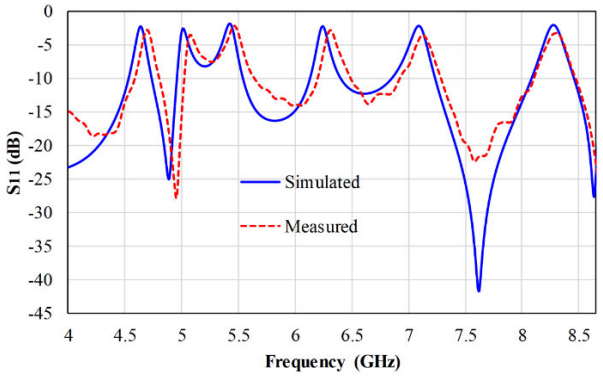

(b)

FIGURE 8. Simulated and observed S_{21} and S_{11} responses of the proposed tag (state: $f_7f_{13}f_{19}f_{28}f_{38}f_{48}$).

To begin with, the first technique is applied. Under its effect, each of the two 8-state identical resonators are combined together to provide a total of 37 states ($2^{5.21}$). 6 resonators (3 combinations of 2 identical resonators) of the suggested structure are designed and implemented. The two identical resonators share 8 resonance frequencies. The first pair of resonators shares the frequencies f_1 to f_8, as shown in Table 4. The second pair of resonators shares the frequencies from f_9 to f_{16} and the third pair shares the frequencies from f_{17} to f_{24}. The designed code in this demonstration corresponds to the resonance frequencies $f_1f_4f_{11}f_{14}f_{21}f_{24}$. The structure occupies the range of the bandwidth from 4.42 GHz to 6.91 GHz. Therefore, the proposed technique increases the spectral density from 1 bit/290 MHz to 1 bit/160 MHz. A photograph of the fabricated circuit is presented in Fig. 5.

It should be noted that, the resonators are spaced in a way to avoid any loading effect, and so any frequency shift when different arms are connected to the coupled line.

The two-port S-parameter measurements were conducted using an Anritsu microwave Vector Network Analyzer (VNA 37369C). Fig. 6 records the simulated and measured insertion loss (S_{21}) and the return loss (S_{11}) of the fabricated configuration. The observed resonance frequencies of this code were $f_1 = 4.42$ GHz, $f_4 = 4.66$ GHz, $f_{11} = 5.30$ GHz, $f_{14} = 5.67$ GHz, $f_{21} = 6.41$ GHz, and $f_{24} = 6.91$ GHz.

The second technique suggested in the paper is implemented using unequal arm-lengths in order to decrease the difference between the adjacent resonance frequencies to approximately 70 MHz instead of approximately 100 MHz. Two 6-resonator circuits with two different codes are designed and implemented. Photographs of these circuits are presented in Fig. 7. The simulated and observed S_{21} and S_{11} responses for these two circuits are summarized in Figs. 8 and 9. The resonance frequencies are denoted by the identifiers f_1 to f_{48} and occupy the bandwidth spectrum from 4.7 GHz to 8.3 GHz. The first circuit is designed for the code $f_7f_{13}f_{19}f_{28}f_{38}f_{48}$ and the second circuit is designed for the code $f_8f_{14}f_{20}f_{29}f_{35}f_{41}$. In this case, the spectral density improves from 1 bit/290 MHz to 1 bit/200 MHz. Further improvement can be achieved by mixing the two aforementioned techniques to produce an expected spectral density that is better than 1 bit/120 MHz.

IV. CHIPLESS RFID TAG DESIGN

Two typical UWB monopole antennas covering the frequency range of 4 to 9 GHz were designed and fabricated to experimentally verify the performance of the proposed tag. The antenna configuration (top-bottom) and its S_{11} responses are shown in Fig. 10. A measurement setup was established to validate the proposed chipless RFID tag, as shown in Fig. 11. The RFID reader system included a vector network analyser (Agilent N9925A) and two UWB horn antennas. The measured tag was placed at a distance of 40 cm from the horn apertures. The setup was equipped with two UWB horn

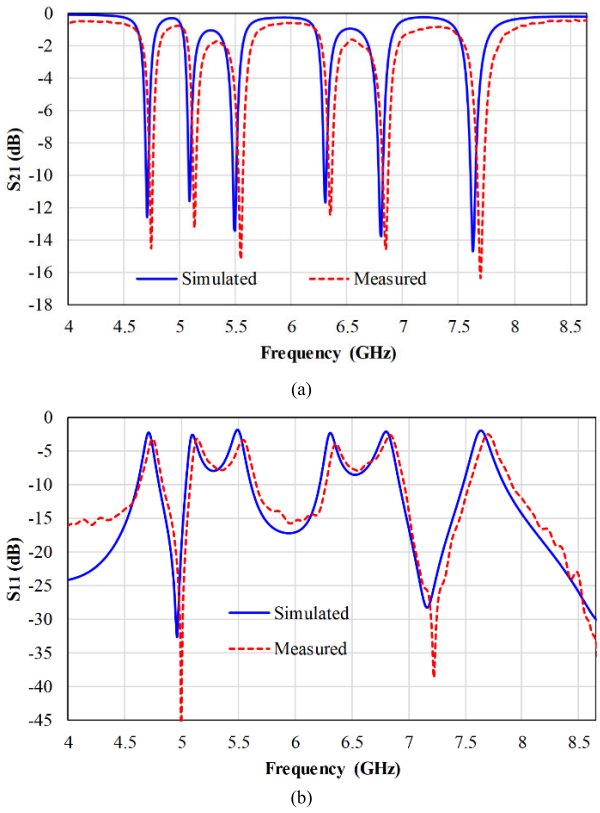

FIGURE 9. Simulated and observed S_{21} and S_{11} responses of the proposed tag (state: $f_8f_{14}f_{20}f_{29}f_{35}f_{41}$).

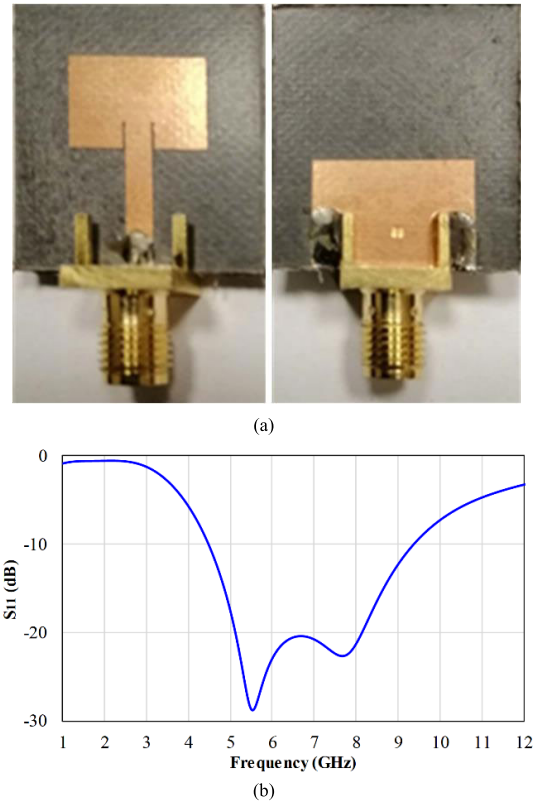

FIGURE 10. (a) UWB antenna geometry and (b) reflection coefficient.

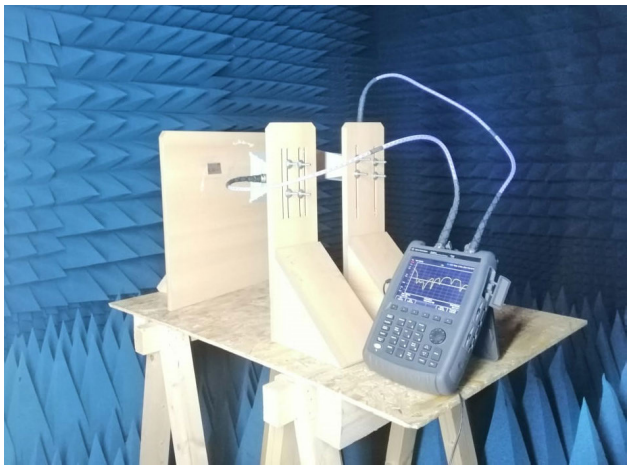

FIGURE 11. Measurement setup for tag testing.

antennas with operational bandwidths from 1 to 18 GHz. All measurements were performed inside the anechoic chamber.

Based on the circuits fabricated and discussed in the previous section, three complete tags were designed and implemented, in which cross-polarized antennas were integrated at the opposite ends of the resonator circuits. The first tag, as shown in Fig. 12, is based on the 6 resonators presented in Fig. 5, in which each pair of resonators shares the same bandwidth. The observed S_{21} magnitudes for the chipless RFID tag are recorded in Fig. 13. The second and third tags, as shown in Fig. 14, are based on the resonator circuits presented in Fig. 7 with the same codes. The measured S_{21} magnitudes of these tags are recorded in Figs. 15 and 16.

Additionally, the group delay is also measured and used to identify the bit positions. As is evident from the data presented in the figures, the observed and simulated results corresponded closely to one another, despite slight discrepancies in certain resonance frequencies. Furthermore, the identification of the position of each bit is very clear from the magnitude and group delay measurements.

The performance parameters of this tag are calculated as follows: spectral capacity (4.39 bits/GHz), spatial density (1.07 bits/cm^2), spatial density at the centre frequency (24.66 bits/λ^2), encoding capacity (0.3 bits/cm^2/GHz), and encoding capacity at the centre frequency (6.01 bits/λ^2/GHz). These performances can be improved by either increasing the number of states per resonator or by the techniques described in the previous section. The first structure is developed by the same configuration shown in Fig. 14, but in this case the number of states per resonator is selected to be $K = 12$. The designed structure, shown in Fig. 17, is optimized in order to maintain the same frequency band and approximately the same area. This has been achieved by decreasing the microstrip lines widths of the resonators. The frequency difference between the two adjacent resonances ranges from 50 MHz to 70 MHz. This structure provides 12^6 codes, or equivalently approximately 21.5 bits. The other

TABLE 5. Performance parameters of the proposed structures.

The proposed technique	Number of resonators (N)	Number of states (K)	Frequency band (GHz)	Capacity (bits)	Spectral capacity (bits/GHz)	Spatial density (bits/cm^2)	Spatial density at the centre frequency (bits/λ^2)	Encoding capacity (bits/cm^2/GHz)	Encoding capacity at the centre frequency (bits/λ^2/GHz)	Size (mm^2)
Un equally arms (Fig. 14)	6	8	4.2-8.3	18	4.39	1.07	24.66	0.30	6.01	54.51×30.92
Same bandwidth shared between two identical resonators (Fig. 19)	12			31.26	7.62	1.31	30.06	0.36	7.33	77.34×30.92
Un equally arms (Fig. 20)	6	12	4.3-8.4	21.51	5.25	1.32	29.51	0.32	7.20	53.37×30.44
Same bandwidth shared between two identical resonators	12			37.82	9.23	1.60	35.73	0.39	8.71	77.51×30.44

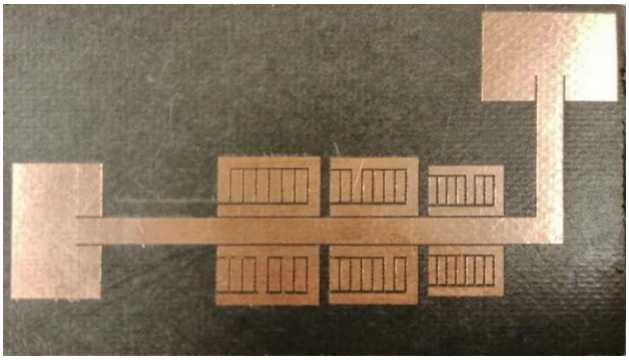

FIGURE 12. Integrated chipless RFID tag prototype (state: $f_1f_4f_{11}f_{14}f_{21}f_{24}$).

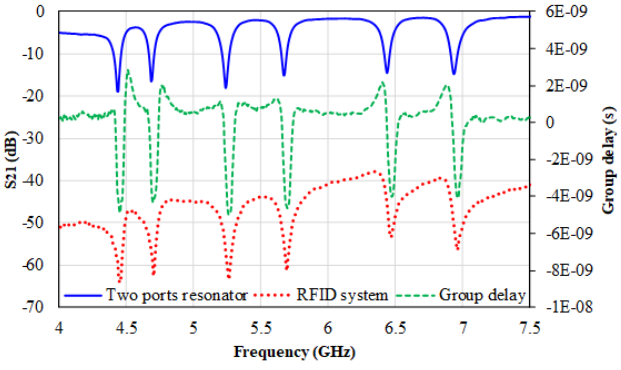

FIGURE 13. Measured magnitude and group delay for the RFID tag ($f_1f_4f_{11}f_{14}f_{21}f_{24}$).

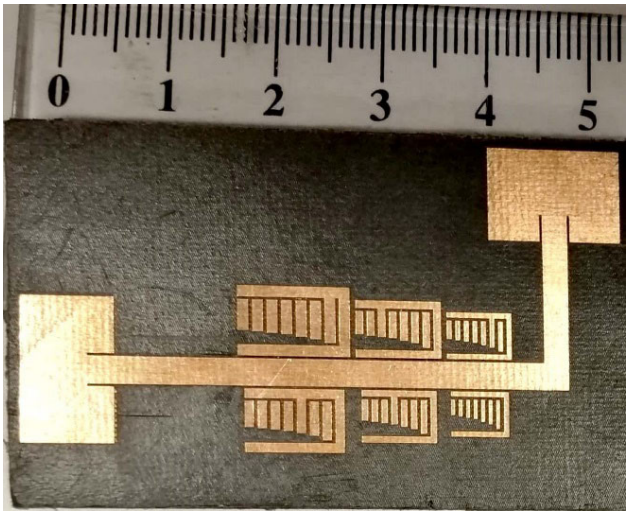

(a)

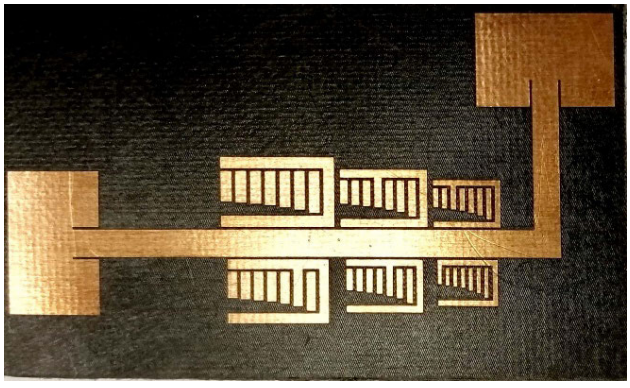

(b)

FIGURE 14. Photographic copies of the proposed tag (a) state: $f_7f_{13}f_{19}f_{28}f_{38}f_{48}$ and (b) state: $f_8f_{14}f_{20}f_{29}f_{35}f_{41}$).

performance parameters are calculated as follows: spectral capacity (5.25 bits/GHz), spatial density (1.32 bits/cm^2), spatial density at the centre frequency (29.51 bits/λ^2), encoding capacity (0.32 bits/cm^2/GHz), and encoding capacity at the centre frequency (7.20 bits/λ^2/GHz). Fig. 18 shows the simulated S_{21} for four different codes.

To further improve the performance, a second structure is designed based on the techniques described in Section 3 by allowing the same bandwidth to be shared between two

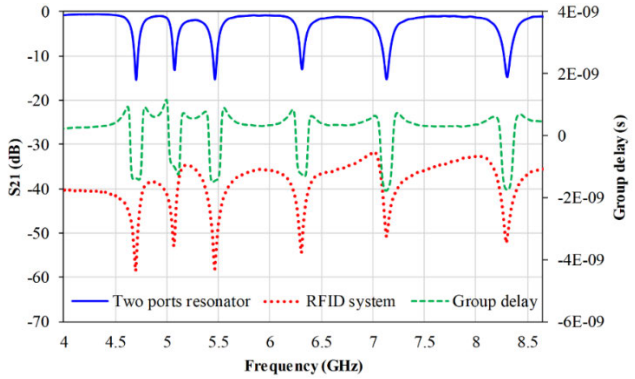

FIGURE 15. Measured magnitudes and group delays for the RFID tag ($f_7f_{13}f_{19}f_{28}f_{38}f_{48}$).

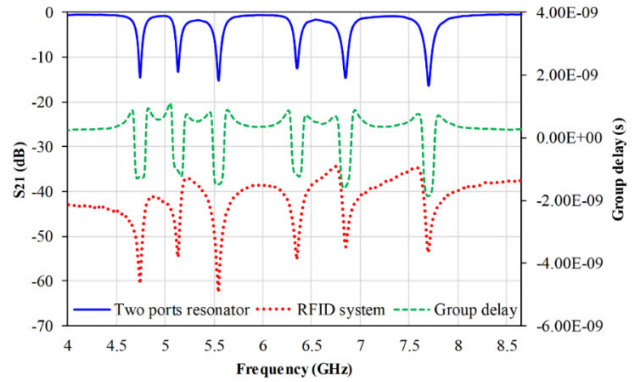

FIGURE 16. Measured magnitudes and group delays for the RFID tag ($f_8f_{14}f_{20}f_{29}f_{35}f_{41}$).

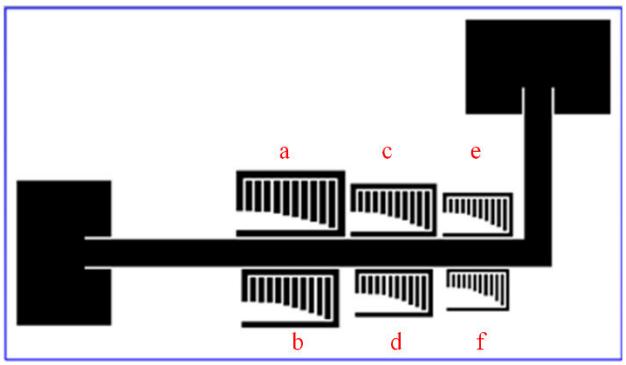

FIGURE 17. 12-state chipless RFID tag geometry (state: $f_1f_{17}f_{25}f_{37}f_{49}f_{61}$).

identical resonators. The design is the same as that presented Fig. 14, but in this case each resonator is used twice. The new structure is shown in Fig. 19. The structure consists of 12 resonators and each two identical resonators have 37 states. Therefore, the 12 resonators provide 6^{37} codes or equivalently approximately 31.3-bit. Significantly, the performance improvement is achieved by this configuration. The performances are calculated as follows: spectral capacity (7.62 bits/GHz), spatial density (1.31 bits/cm^2), spatial density at the centre frequency (30.06 bits/λ^2), encoding capacity (0.36 bits/cm^2/GHz), and encoding capacity at the centre

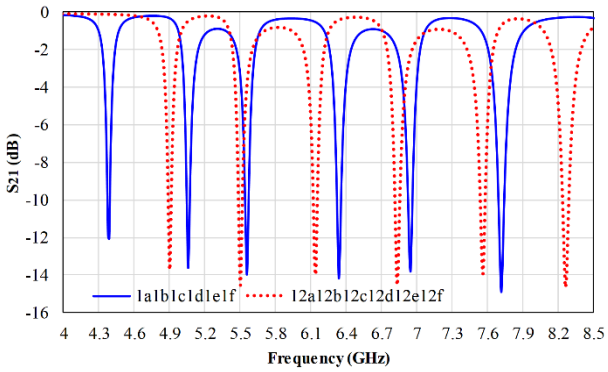

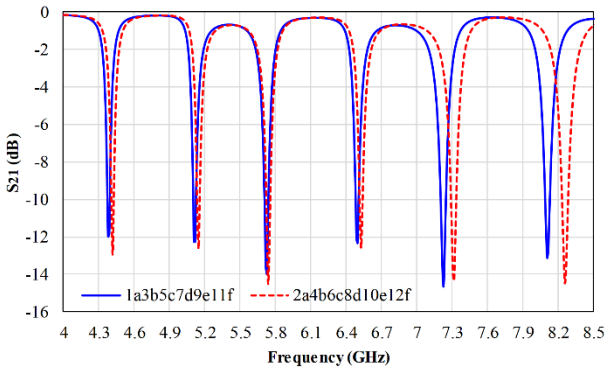

FIGURE 18. Simulated S_{21} for six 12-state resonators (a) states: ($f_1f_{17}f_{25}f_{37}f_{49}f_{61}$), and ($f_{12}f_{24}f_{36}f_{48}f_{60}f_{72}$) and (b) states: ($f_1f_{19}f_{29}f_{43}f_{57}f_{71}$), and ($f_2f_{20}f_{30}f_{44}f_{58}f_{72}$).

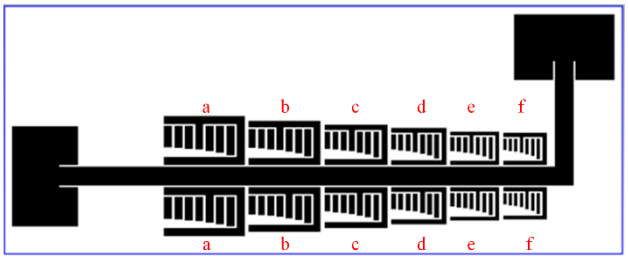

FIGURE 19. Geometry for the proposed RFID tag when the same bandwidth is shared between two identical resonators (with K = 8, and N = 12).

frequency (7.33 bits/λ^2/GHz). Fig. 20 shows the simulated S_{21} for four different codes.

If two identical resonators shared the same bandwidth and the number of states increased to K = 12, then each two identical resonators provide 79 states ($2^{7.17}$). Therefore, the 12 resonators provide 6^{79} codes or equivalently approximately 37.8-bit. This configuration significantly improves the performance.

The performances are calculated as follows: spectral capacity (9.23 bits/GHz), spatial density (1.60 bits/cm^2), spatial density at the centre frequency (35.73 bits/λ^2), encoding capacity (0.39 bits/cm^2/GHz), and encoding capacity at the centre frequency (8.71 bits/λ^2/GHz). Table 5 summarize the performance comparisons between these proposed techniques.

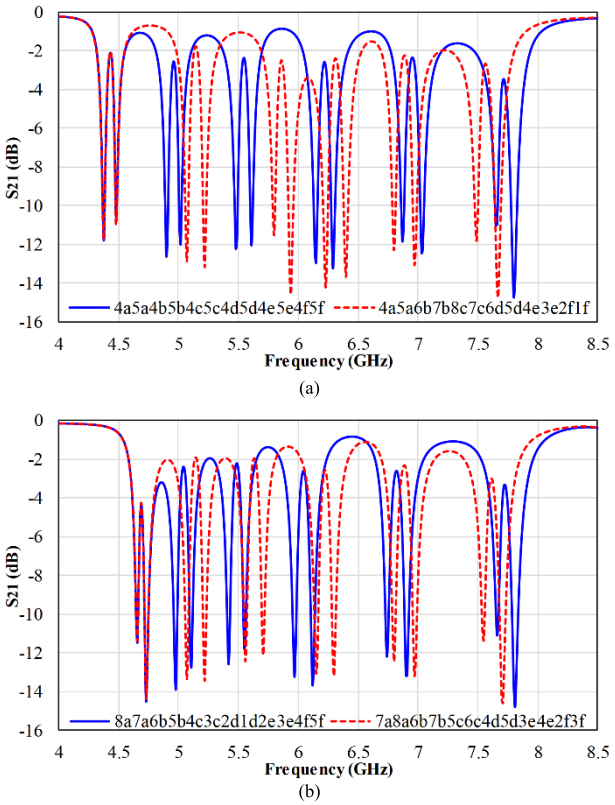

FIGURE 20. Simulated S_{21} for six 8-state resonators (a states: $(f_4f_5f_{12}f_{13}f_{20}f_{21}f_{28}f_{29}f_{36}f_{37}f_{44}f_{45})$, and $(f_4f_5f_{14}f_{15}f_{24}f_{23}f_{30}f_{29}f_{36}f_{35}f_{42}f_{41})$ and (b) states: $(f_8f_7f_{14}f_{13}f_{20}f_{19}f_{26}f_{25}f_{34}f_{35}f_{44}f_{45})$, and $(f_7f_8f_{14}f_{15}f_{21}f_{22}f_{28}f_{29}f_{35}f_{36}f_{42}f_{43})$.

V. CONCLUSION

A new compact reconfigurable K-state resonator suitable for chipless RFID tags was presented. This allows each resonator to represent more than one bit of information.

The structure has the advantages of increasing the tag's capacity without increasing the number of resonators, while simultaneously simplifying the detection process. Therefore, the proposed structure allows a large amount of data to be stored in a compact space in order to reduce the cost of storage per bit. Two techniques are also presented that permit improving the spectral efficiency. The first technique is achieved by allowing each two resonators to share the same bandwidth.

The second technique is performed by optimizing the structure in order to reduce the difference between adjacent resonance frequencies to be approximately 70 MHz and to maintain the ability of clearly reading any code. Several tags for codes with K = 8 (3 bits/resonator) are designed and implemented on the RT Duroid 5880 substrate as a proof-of-concept. Each resonator can be implemented in an area that is almost the same size as the area of a conventional 2-state resonator. A satisfactory agreement between the empirical and simulated results is confirmed.

REFERENCES

[1] S. Preradovic and N. C. Karmakar, *Multiresonator-Based Chipless RFID: Barcode of the Future*. New York, NY, USA: Springer, 2012.

[2] R. Rezaiesarlak and M. Manteghi, *Chipless RFID: Design Procedure and Detection Techniques*. New York, NY, USA: Springer, 2014.

[3] M. Pöpperl, A. Parr, C. Mandel, R. Jakoby, and M. Vossiek, "Potential and practical limits of time-domain reflectometry chipless RFID," *IEEE Trans. Microw. Theory Techn.*, vol. 64, no. 9, pp. 2968–2976, Sep. 2016.

[4] S. Genovesi, F. Costa, A. Monorchio, and G. Manara, "Chipless RFID tag exploiting multifrequency delta-phase quantization encoding," *IEEE Antennas Wireless Propag. Lett.*, vol. 15, pp. 738–741, 2015.

[5] A. Jiménez-Sáez, M. Schüßler, M. Nickel, and R. Jakoby, "Hybrid time-frequency modulation scheme for chipless wireless identification and sensing," *IEEE Sensors J.*, vol. 18, no. 19, pp. 7850–7859, Oct. 2018.

[6] M. A. Islam and N. C. Karmakar, "Real-world implementation challenges of a novel dual-polarized compact printable chipless RFID tag," *IEEE Trans. Microw. Theory Techn.*, vol. 63, no. 12, pp. 4581–4591, Dec. 2015.

[7] C. Herrojo, J. Mata-Contreras, A. Núñez, F. Paredes, E. Ramon, and F. Martín, "Near-field chipless-RFID system with high data capacity for security and authentication applications," *IEEE Trans. Microw. Theory Techn.*, vol. 65, no. 12, pp. 5298–5308, Dec. 2017.

[8] F. Babaeian and N. C. Karmakar, "Hybrid chipless RFID tags—A pathway to EPC global standard," *IEEE Access*, vol. 6, pp. 67415–67426, 2018.

[9] L. M. Arjomandi, G. Khadka, Z. Xiong, and N. C. Karmakar, "Document verification: A cloud-based computing pattern recognition approach to chipless RFID," *IEEE Access*, vol. 6, pp. 78007–78015, 2018.

[10] A. Vena, E. Perret, and S. Tedjini, "A fully printable chipless RFID tag with detuning correction technique," *IEEE Microw. Wireless Compon. Lett.*, vol. 22, no. 4, pp. 209–211, Apr. 2012.

[11] S. Tedjini, N. Karmakar, E. Perret, A. Vena, R. Koswatta, and R. E-Azim, "Hold the chips: Chipless technology, an alternative technique for RFID," *IEEE Microw. Mag.*, vol. 14, no. 5, pp. 56–65, Jul./Aug. 2013.

[12] M. A. Islam and N. C. Karmakar, "Compact printable chipless RFID systems," *IEEE Trans. Microw. Theory Techn.*, vol. 63, no. 11, pp. 3785–3793, Nov. 2015.

[13] M. Svanda, M. Polivka, J. Havlicek, and J. Machac, "Chipless RFID tag with an improved magnitude and robustness of RCS response," *Microw. Opt. Techn. Lett.*, vol. 59, no. 2, pp. 488–492, Feb. 2017.

[14] W. M. Abdulkawi, A.-F. A. Sheta, K. Issa, and S. A. Alshebeili, "Compact printable inverted-M shaped chipless RFID tag using dual-polarized excitation," *Electronics*, vol. 8, no. 5, p. 580, 2019, doi: 10.3390/electronics8050580.

[15] M. Polivka, J. Havlicek, M. Svanda, and J. Machac, "Improvement in robustness and recognizability of RCS response of U-shaped strip-based chipless RFID tags," *IEEE Antennas Wireless Propag. Lett.*, vol. 15, pp. 2000–2003, 2016.

[16] M. Svanda, J. Havlicek, J. Machac, and M. Polivka, "Polarisation independent chipless RFID tag based on circular arrangement of dual-spiral capacitively-loaded dipoles with robust RCS response," *IET Microw., Antennas Propag.*, vol. 12, no. 14, pp. 2167–2171, 2018, doi: 10.1049/iet-map.2018.5434.

[17] L. Wang, C. Hu, X. Wu, Z. Xia, and W. Wen, "Multi-band metamaterial absorber with arbitrary polarization and wide-incident angle," *Appl. Phys. A, Solids Surf.*, vol. 123, no. 10, p. 651, Oct. 2017.

[18] S. Fan, T. Chang, X. Liu, Y. Fan, and M. M. Tentzeris, "A depolarizing chipless RFID tag with humidity sensing capability," in *Proc. IEEE Int. Symp. Antennas Propag. USNC/URSI Nat. Radio Sci. Meeting*, Jul. 2018, pp. 2469–2470.

[19] F. Deng, Y. He, B. Li, Y. Song, and X. Wu, "Design of a slotted chipless RFID humidity sensor tag," *Sens. Actuators B, Chem.*, vol. 264, pp. 255–262, Aug. 2018.

[20] I. Preradovic, I. Balbin, N. C. Karmakar, and G. F. Swiegers, "Multiresonator-based chipless RFID system for low-cost item tracking," *IEEE Trans. Microw. Theory Techn.*, vol. 57, no. 5, pp. 1411–1419, May 2009.

[21] S. Preradovic, S. Roy, and N. Karmakar, "Fully printable multi-bit chipless RFID transponder on flexible laminate," in *Proc. Asia–Pacific Microw. Conf.*, Dec. 2009, pp. 2371–2374, doi: 10.1109/APMC.2009.5385460.

[22] S. Preradovic and N. C. Karmakar, "Chipless RFID: Bar code of the future," *IEEE Microw. Mag.*, vol. 11, no. 7, pp. 87–97, Dec. 2010.

[23] P. Prabavathi and S. S. Rani, "Design of frequency-signature based multiresonators using quarter wavelength open ended stub for chipless RFID tag," in *Proc. Nat. Conf. Commun. (NCC)*, Feb. 2019, pp. 1–6, doi: 10.1109/NCC.2019.8732229.

[24] O. Rance, R. Siragusa, P. Lemaître-Auger, and E. Perret, "Toward RCS magnitude level coding for chipless RFID," *IEEE Trans. Microw. Theory Techn.*, vol. 64, no. 7, pp. 2315–2325, Jul. 2016.

[25] A. M. J. Marindra and G. Y. Tian, "Chipless RFID sensor tag for metal crack detection and characterization," *IEEE Trans. Microw. Theory Techn.*, vol. 66, no. 5, pp. 2452–2462, May 2018.
[26] M. A. Bibile and N. C. Karmakar, "Moving chipless RFID tag detection using adaptive wavelet-based detection algorithm," *IEEE Trans. Antennas Propag.*, vol. 66, no. 6, pp. 2752–2760, Jun. 2018.
[27] Y. J. Zhang, R. X. Gao, Y. He, and M. S. Tong, "Effective design of microstrip-line chipless RFID tags based on filter theory," *IEEE Trans. Antennas Propag.*, vol. 67, no. 3, pp. 1428–1436, Nov. 2018.
[28] M. A. Islam and N. C. Karmakar, "A novel compact printable dual-polarized chipless RFID system," *IEEE Trans. Microw. Theory Techn.*, vol. 60, no. 7, pp. 2142–2151, Jul. 2012.
[29] W. M. Abdulkawi and A.-F. A. Sheta, "Design of chipless RFID tag based on stepped impedance resonator for IoT applications," in *Proc. Int. Conf. Innov. Intell. Inform., Comput., Technol. (3ICT)*, Nov. 2018, pp. 1–4, doi: 10.1109/3ict.2018.8855730.
[30] W. M. Abdulkawi and A.-F. A. Sheta, "Four-state coupled-line resonator for chipless RFID tags application," *Electronics*, vol. 8, no. 5, p. 581, 2019, doi: 10.3390/electronics8050581.
[31] C. M. Nijas, R. Dinesh, U. Deepak, A. Rasheed, S. Mridula, K. Vasudevan, and P. Mohanan, "Chipless RFID tag using multiple microstrip open stub resonators," *IEEE Trans. Antennas Propag.*, vol. 60, no. 9, pp. 4429–4432, Sep. 2012.
[32] M. A. Ashraf, Y. A. Alshoudokhi, H. M. Behairy, M. R. Alshareef, S. A. Alshebeili, K. Issa, and H. Fathallah, "Design and analysis of multi-resonators loaded broadband antipodal tapered slot antenna for chipless RFID applications," *IEEE Access*, vol. 5, pp. 25798–25807, 2017, doi: 10.1109/ACCESS.2017.2768118.
[33] V. Sharma and M. Hashmi, "Chipless RFID tag based on open-loop resonator," in *Proc. IEEE Asia–Pacific Microw. Conf. (APMC)*, Nov. 2017, pp. 543–546.
[34] A. A. C. Alves, D. H. Spadoti, and L. L. Bravo-Roger, "Optically controlled multiresonator for passive chipless tag," *IEEE Microw. Wireless Compon. Lett.*, vol. 28, no. 6, pp. 467–469, Jun. 2018, doi: 10.1109/lmwc.2018.2824726.
[35] W. M. Abdulkawi and A. A. Sheta, "Printable chipless RFID tags for IoT applications," in *Proc. ICCAIS*, Apr. 2018, pp. 1–4, doi: 10.1109/cais.2018.8441955.
[36] Z. Ma and C.-C. Chen, "A hybrid coding retransmitted chipless tag loaded by microstrip resonator," *Microelectron. Rel.*, vol. 93, pp. 1–7, Feb. 2019.
[37] Z.-H. Ma, J.-H. Yang, C.-C. Chen, and C.-F. Yang, "A re-transmitted chipless tag using CSRR coupled structure," *Microsyst. Technol.*, vol. 24, no. 10, pp. 4373–4382, 2018.
[38] S. Preradovic and N. C. Karmakar, "Design of fully printable planar chipless RFID transponder with 35-bit data capacity," in *Proc. IEEE Eur. Microw. Conf. (EuMC)*, Sep. 2009, pp. 13–16.
[39] S. Preradovic and N. C. Karmakar, "Design of chipless RFID tag for operation on flexible laminates," *IEEE Antennas Wireless Propag. Lett.*, vol. 9, pp. 207–210, 2010, doi: 10.1109/lawp.2010.2045872.
[40] W. M. Adbulkawi and A. A. Sheta, "A compact chipless RFID tag based on frequency signature," in *Proc. 9th IEEE-GCC Conf. Exhib. (GCCCE)*, May 2017, pp. 1–4.
[41] W. M. Abdulkawi and A. F. A. Sheta, "Multi-resonator structure for small size chipless radio frequency identification tag," *Int. J. Comput. Digit. Syst.*, vol. 7, no. 1, pp. 43–49, 2018.
[42] C. Herrojo, J. Naqui, F. Paredes, and F. Martín, "Spectral signature barcodes based on S-shaped split ring resonators (S-SRRs)," *EPJ Appl. Metamater.*, vol. 3, p. 1, Jun. 2016.
[43] C. Herrojo, F. Paredes, J. Mata-Contreras, S. Zuffanelli, and F. Martín, "Multistate multiresonator spectral signature barcodes implemented by means of S-shaped split ring resonators (S-SRRs)," *IEEE Trans. Microw. Theory Techn.*, vol. 65, no. 7, pp. 2341–2352, Jul. 2017.
[44] W. M. Abdulkawi and A. A. Sheta, "High coding capacity chipless radiofrequency identification tags," *Microw. Opt. Technol. Lett.*, to be published.
[45] I. Balbin and N. C. Karmakar, "Phase-encoded chipless RFID transponder for large-scale low-cost applications," *IEEE Microw. Wireless Compon. Lett.*, vol. 19, no. 8, pp. 509–511, Aug. 2009.
[46] A. Vena, E. Perret, and S. Tedjini, "Chipless RFID tag using hybrid coding technique," *IEEE Trans. Microw. Theory Techn.*, vol. 59, no. 12, pp. 3356–3364, Dec. 2011.
[47] A. Vena, E. Perret, and S. Tedjini, "A compact chipless RFID tag using polarization diversity for encoding and sensing," in *Proc. IEEE Int. Conf. RFID (RFID)*, Apr. 2012, pp. 191–197.
[48] Y.-Z. Ni, X.-D. Huang, Y.-P. Lv, and C.-H. Cheng, "Hybrid coding chipless tag based on impedance loading," *IET Microw., Antennas Propag.*, vol. 11, no. 10, pp. 1325–1331, Aug. 2017.
[49] C. Herrojo, J. Mata-Contreras, F. Paredes, A. Núñez, E. Ramon, and F. Martín, "Near-field chipless-RFID system with erasable/programmable 40-bit tags inkjet printed on paper substrates," *IEEE Microw. Wireless Compon. Lett.*, vol. 28, no. 3, pp. 272–274, Mar. 2018.
[50] F. Sakai, M. Makimoto, and K. Wada, "Multimode stepped impedance resonators and their application in chipless RFID tags," in *Proc. IEEE 46th Eur. Microw. Conf. (EuMC)*, Oct. 2016, pp. 604–607.
[51] M. Makimoto and F. Sakai, "Multimode resonator and RFID tags using the same," U.S. Patent 9 537 194, Mar. 1, 2017.
[52] M. Svanda, M. Polivka, J. Havlicek, J. Machac, and D. H. Werner, "Platform tolerant, high encoding capacity dipole array-plate chipless RFID tags," *IEEE Access*, vol. 7, pp. 138707–138720, 2019.
[53] K. Mc Gee, P. Anandarajah, and D. Collins, "A review of chipless remote sensing solutions based on RFID technology," *Sensors*, vol. 19, no. 22, p. 4829, 2019.
[54] W. M. A. Abdulkawi and A. F. A. Sheta, "Reconfigurable resonators for chipless RFID applications," U.S. Patent 15 974 588, Feb. 19, 2019.
[55] S. Gupta, G. J. Li, R. C. Roberts, and L. J. Jiang, "Log-periodic dipole array antenna as chipless RFID tag," *Electron. Lett.*, vol. 50, no. 5, pp. 339–341, Feb. 2014.
[56] M. Khaliel, A. El-Awamry, A. F. Megahed, and T. Kaiser, "A novel design approach for co/cross-polarizing chipless RFID tags of high coding capacity," *IEEE J. Radio Freq. Identificat.*, vol. 1, no. 2, pp. 135–143, Jun. 2017.
[57] V. Sharma, S. Malhotra, and M. Hashmi, "Slot resonator based novel orientation independent chipless RFID tag configurations," *IEEE Sensors J.*, vol. 19, no. 13, pp. 5153–5160, Jul. 2019.
[58] M. A. Islam, M. S. Bhuiyan, and N. Karmakar, "A novel compact chipless RFID tag and near-field reader," in *Proc. Asia–Pacific Microw. Conf. Proc. (APMC)*, Dec. 2011, pp. 1518–1521.
[59] M. A. Islam, Y. Yap, and N. Karmakar, "'△' slotted compact printable orientation insensitive chipless RFID tag for long range applications," in *Proc. 9th Int. Conf. Electr. Comput. Eng. (ICECE)*, Dec. 2016, pp. 283–286, doi: 10.1109/ICECE.2016.7853911.

WAZIE M. ABDULKAWI received the B.S. degree in electrical communication engineering from Ibb University, Ibb, Yemen, in 2007, and the M.S. degree in electrical engineering from King Saud University, Riyadh, Saudi Arabia, in 2013, where he is currently pursuing the Ph.D. degree in electrical engineering with the Electrical Engineering Department. His research interests include reconfigurable antennas, chipless RFID tags, planer, and uniplanar MIC's. He also holds a patent for chipless RFID tags.

ABDEL-FATTAH A. SHETA received the B.S. degree in communications and electro-physics from Alexandria University, Egypt, in 1985, the M.S. degree with the Electrical Engineering Department, Cairo University, in 1991, and the Ph.D. degree in microwave circuits analysis and design from the ENST, Université de Bretagne Occidentale, France, in 1996. From 1996 to 1998, he worked as a Researcher with the National Telecommunication Institute, Cairo, Egypt. In 1998, he joined the Electrical Engineering Department, Fayoum University. He is currently a Full Professor with the EE Department, King Saud University, Riyadh, Saudi Arabia. He established a high-tech laser-based microstrip fabrication and integration Lab. He has participated in many research projects funded from the College of Engineering Research Centre and the National Plan for Sciences and Technology (NPST), King Saud University. His current research interests include reconfigurable RF systems, UWB systems, microstrip antennas, antennas for hyperthermia applications, chipless RFID systems, microstrip filters, and planar and uniplanar MIC's, and MMIC's.